



A study on the structural, wear, and corrosion properties of CoCuFeNiMo high-entropy alloy

Sefa Emre Sünbül *

Gaziantep University, Engineering Faculty, Department of Metallurgical and Materials Engineering, Gaziantep 27310, Turkey



ARTICLE INFO

Keywords:
CoCuFeNiMo
High entropy alloys
Wear resistance, corrosion properties

ABSTRACT

This study investigates the structural properties, wear resistance and corrosion behavior of a CoCuFeNiMo equiatomic high-entropy alloy. The alloy was prepared using a vacuum arc melting device, and its structural properties were analyzed through X-ray diffraction (XRD) and scanning electron microscopy (SEM). Wear tests were conducted using a pin-on-disc machine against 4140 stainless steel at different loads. Corrosion behavior was evaluated through potentiodynamic polarization and electrochemical impedance spectroscopy (EIS) in a 3.5 wt% NaCl solution. The results indicated the presence of a major face-centered cubic (FCC) phase and a minor (μ) phase. The alloy exhibited segregation of Cu, attributed to positive mixing enthalpy. The coefficient of friction exhibited stability under lower loads but fluctuated under higher loads, possibly due to inhomogeneity in the microstructure caused by Cu segregation. Wear rates increased linearly with applied loads, indicating a direct relationship between load and wear properties. The worn surfaces displayed characteristics of mild abrasive wear, with delaminations, plowing, and abrasive wear tracks. Pitting corrosion was observed, and the corrosion process was explained as the attack of Cl^- ions leading to galvanic corrosion between different phases. In the corrosion analysis, the E_{corr} value was -0.616 V, and the i_{corr} value was found to be 2.22×10^{-5} A/cm².

1. Introduction

The first high-entropy alloys were created by Cantor et al. [1] as CoCrFeNiMn and by Yeh et al. [2] as CoCrCuFeNiAl_x. As a matter of fact, CoCrFeNiMn has been mentioned in the literature as a Cantor alloy [3]. The presence of Cr in the structure can generally form a brittle intermetallic σ phase [3,4]. There are various reasons for both favouring and disfavoring the Cu element. The role of Cu in high entropy alloys remains unclear [5]. While some studies do not prefer Cu because it causes segregation and accumulation, which is reported to reduce hardness and wear, other studies prefer Cu because it favors this segregation and deposition and improves oxidation and some other properties [3,5]. This segregation or decomposition of Cu is due to the positive mixing enthalpy. Furthermore, copper (Cu) serves as a robust stabilizer for the face-centered cubic (FCC) structure [6]. Additionally, the lower melting temperature of Cu compared to other elements allows for a reduction in the processing temperature of the alloys. The addition of Cu can often form secondary phases such as Cu-rich FCC, L1₂ [3,6]. The quaternary CoCuFeNi high-entropy alloy formed by removing Cr and adding Cu is a kind of alloy with a single-phase FCC phase, which can have excellent

properties for use in semiconductor devices, spacecraft engine components, heat exchangers and navigation equipment [7–9]. On the contrary, the CoCuFeNi high entropy alloy is capable of forming two face-centered cubic (FCC) phases: one rich in (Co, Fe, and Ni) and the other rich in Cu. It exhibits a relatively high yield strength compared to the CoCrFeNi high entropy alloy, attributed to the presence of a phase boundary [3,8,10]. Additional elements, such as Al, Mn, Mo, and Nb, are frequently introduced into high entropy alloys to enhance their strength, hardness, corrosion resistance, and tribological and fatigue properties [8]. Notably, molybdenum (Mo), characterized by a relatively large atomic radius and high modulus, serves as an effective solid solution strengthening element. It plays a role in grain refinement, imparts thermal strength, and simultaneously enhances the ductility, toughness, and wear resistance of the alloy [11].

Kumar et al.'s study [12] mentioned that high entropy alloys (HEAs) can be used in applications such as biomaterial, aerospace, and electronic industries because they have already proven better tribological and corrosion resistance than conventional alloys. In addition, it has been reported that they can be produced with different fabrication techniques, and their properties can be improved with surface

* Correspondence to: Gaziantep University, Department of Metallurgical and Materials Engineering, Gaziantep 27310, Turkey.
E-mail address: sunbulsefa@ktu.edu.tr.

treatments such as coatings. In the study by Xiao et al. [13], TiZrHfNb-based RHEAs were prepared by adding Mo and Ta and their phases, microstructures and hardness were examined. Additionally, tribocorrosion behaviors against Si₃N₄ balls in 3.5 wt% NaCl solution were investigated and compared with dry sliding. The results show that TiZrHfNb-based RHEAs have a single BCC structure, and the hardness increases with lattice distortion. The addition of Ta and Mo to TiZrHfNb-based RHEAs can effectively improve the corrosion and wear resistance, which is attributed to the formation of passivation film and increased hardness. In a study for marine application [14], the Vickers hardness and compressive yield strength of the AlCoCrFeNi high-entropy alloy, which can be an alternative to 2205 duplex stainless steel and Incoloy 825 alloys, are ~517.6 HV and ~1306.4 MPa, respectively. It has also been found that AlCoCrFeNi HEA has better resistance to wear and corrosion damage compared to 2205 DSS and Incoloy 825 alloys. In a study examining the effect of Cu dispersion on the tribocorrosion mechanisms of CoCrFeNiCu_{0.3} high entropy alloys [15], it was found that the progressive dissolution of the copper element leads to an increase in the friction coefficient of the alloy, which in turn leads to a decrease in the wear rate. Optimization of the distribution of copper from segregation to homogeneity effectively increased the tribo-corrosion resistance of the alloys. Sun et al. [16] studied the effects of Sc content on microstructure, hardness, wear and corrosion resistance in Al1.2CoCrFeNiSc_x high entropy alloys. The results showed that the addition of Sc promoted the formation of the FCC phase and improved the hardness and wear resistance but reduced the corrosion resistance of the alloy. Wang et al. [17] studied the tribocorrosion behavior of FeCrNiCo, FeCrNiCoAl and FeCrNiCoMo high entropy alloys in artificial seawater. Since Al dissolves preferentially, FeCrNiCoAl alloy has a small coefficient of friction and a large wear rate. The wear rate of the FeCr-NiCoMo alloy is lowest due to wear debris containing molybdate fillings in the corrosion pits where the FCC phase corrodes first. Miao et al. [18, 19] have found that AlCoCrFeNi_{2.1} high entropy alloy maintains high hardness (>197 HV) up to 900 °C. The wear rates of the alloy increased monotonically from room temperature to 900 °C, while the friction coefficient decreased sharply when exceeding 600 °C. Ge et al. [20] prepared AlCoCrFeNiTa_x high-entropy alloys by vacuum arc melting method and applied laser remelting process to regulate the microstructure. The AlCoCrFeNiTa_x alloys had typical dendritic morphology, and the addition of Ta element promoted the formation of the Laves phase, gradually changing the alloys from two phases (BCC + B2) to three phases (BCC + B2 + Laves phase). Hardness and wear resistance of AlCoCrFeNiTa_x alloys improved by increasing Ta content.

In the literature, there is only one study on the microstructural and mechanical properties of (CoCuFeNi)_{100-x}Mo_x (x = 0, 10, 15, 19, and 25, at%) alloys [8]. In this study, only equiatomic CoCuFeNiMo alloy was formed by removing Cr and Mn from CoCrFeNiMn (Cantor alloy) and adding Cu and Mo instead. CoCuFeNiMo equiatomic alloy is produced using the arc melting method, and the structural, microhardness wear, and corrosion properties of the alloy are investigated. The objective of this study is to investigate the wear and corrosion resistance of CoCu-FeNiMo alloy in order to expand its application in the industry and provide support/information for this field.

2. Materials and methods

CoCuFeNiMo equiatomic alloy was prepared by a vacuum arc melting device of high-purity elements in an Ar atmosphere. The alloy was remelted five times, inverting each time to ensure chemical homogenization. The sample was melted in a water-cooled Cu crucible with a W electrode. In order to examine the structural properties of the sample, it was cut into small pieces. X-ray diffraction (XRD) analysis was performed with the radiation source CuK α radiation in the 2 θ range from 10° to 90° with a step size of 0.013°/s by PANalytical Xpert Powder³ device. After the standard metallographic procedure, the Zeiss EVO LS10 model Scanning electron microscope (SEM) device was used to

image the microstructure and morphologies of worn and corroded surfaces. The ratio of the elements in the phases was detected using a selective area energy dispersive X-ray spectrometry (EDX) analysis. Vickers microhardness was determined across cross-sections with a Qness Q30 hardness tester using 0.1 kgf load and 10 s dwell time. Each hardness value was recorded as the average of 5 measurements at each depth. The wear properties of the alloy were confirmed in contact with 4140 stainless steel at dry condition using a pin-on disc machine. Wear tests were carried out at a sliding speed of 0.3 m/s, a sliding distance of 4000 m, at room temperature and different loads of 12.5 N, 25 N and 50 N. Weight loss was obtained by weighing the samples for all three different loads before and after each test. The wear rate was calculated using the following Eq. (1):

$$(W_s = \frac{\Delta m}{\rho F_n L}) \quad (1)$$

where W_s is wear rate ($\text{mm}^3/\text{N.m}$), Δm is the weight loss (g), ρ is density (g/cm^3), F_n is the applied load (N), and L is the sliding distance (m). To investigate the corrosion properties, Tafel and electrochemical impedance spectroscopy (EIS) measurements were performed using a Gamry Interface 1010E model device. Electrochemical properties were measured using a triple electrode with CoCuFeNiMo high entropy alloy as a working electrode, graphite rod as a counter electrode, and a saturated calomel electrode as the reference electrode. All corrosion experiments were carried out at room temperature in a testing solution containing 3.5 wt% NaCl, and they were conducted for 3600 seconds to achieve a stable open circuit potential. Tafel measurements were carried out on the samples, covering a voltage range from -1.5–1.5 V while maintaining a constant scan rate of 10 mV/s. EIS measurements were made on the produced samples using an AC voltage of 10 mV rms and a frequency range spanning from 10^{-2} Hz to 10^5 Hz.

3. Results and discussion

Fig. 1 shows the XRD pattern of CoCuFeNiMo high entropy alloy, which includes dual FCC1 and FCC2 phases and a minor μ phase. No other peaks or phases could be detected. Dual Cu-poor FCC1 and Cu-rich FCC2 were detected in the Cu_{28.36}Ni_{22.32}Fe_{19.12}Co_{15.17}Cr_{12.26}Mo_{2.77} high entropy alloy prepared by the plasma arc additive manufacturing method in a study [21]. In a study using similar elements [8], the XRD pattern of CoCuFeNi alloy without Mo included only the FCC phase. In addition, in the phases of (CoCuFeNi)_{100-x}Mo_x (x = 10, 15, 19, and 25 at %) alloys [8], it was revealed that the μ phase was formed in addition to the FCC phase, like this study. In the literature, the μ phase has also been

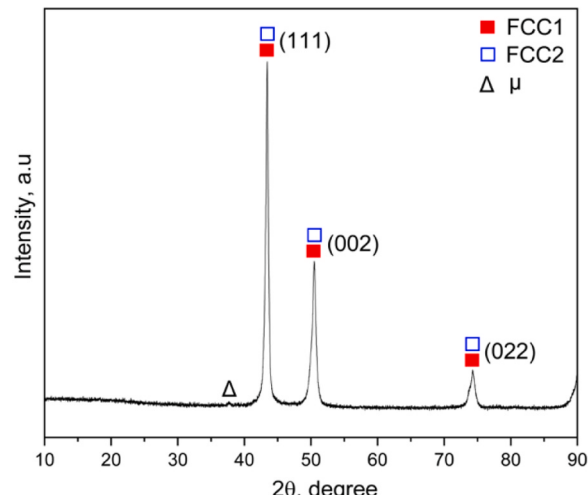


Fig. 1. XRD pattern of CoCuFeNiMo high entropy alloy.

encountered in high-entropy alloys containing Mo [22]. Li et al. [23] produced $\text{Co}_{24}\text{Cr}_{24}\text{Fe}_{24}\text{Ni}_{24}\text{Mo}_4$ alloys by arc melting. They quenched the alloys after homogenization at 1200 °C for 24 h and annealed alloys for 1 hour at 800–1200 °C. They found only the FCC phase in the XRD. In Shun et al. [24]'s study, Mo0 and Mo0.3 alloys among the CoCrFeNiMo_x ($x = 0, 0.3, 0.5$, and 0.85 , in molar ratio) alloys, which were produced by arc melting, have only a single FCC solid solution phase, while the $\text{Mo}_{0.5}$ alloy has σ phase outside the FCC phase. μ phase was detected in addition to the σ phase in $\text{Mo}_{0.85}$ alloy. The structure of the mentioned μ phase is attributed to the rhombohedral Co_7Mo_6 phase. Bae et al. [25] produced alloys with nominal compositions of $\text{Co}_{17.5}\text{Cr}_{12.5}\text{Fe}_{55}\text{Ni}_{10}\text{Mo}_5$ and $\text{Co}_{18}\text{Cr}_{12.5}\text{Fe}_{55}\text{Ni}_7\text{Mo}_{7.5}$ by induction melting. As a result of the annealing process at 900–1200 °C, the μ phase was found in small concentrations in addition to the FCC phase at some temperatures. Unlike this study, Soni et al. [26] found only FCC phases in FeCoNiCuMo_x ($x = 0.2, 0.4, 0.6, 0.8, 1$) alloys.

The microstructure of CoCuFeNiMo high entropy alloys by SEM is shown in Fig. 2. Besides, the EDX-mapping analysis of the alloy presented in Fig. 2 provides insights into the microstructure details and element contributions. The compositions of point EDX analyzes are shown in Fig. 3. As can be seen from Fig. 2 and Fig. 3, Cu decomposes from others. In other words, it has been determined that Cu segregates and does not mix with Co, Fe and Ni in this alloy. The primary explanation for this phenomenon is believed to be the substantial positive mixing enthalpies between copper (Cu) and the other constituent elements. According to point EDX results, spectrum 14, 15 and 17, dark gray regions, are the equally distributed sections (FCC1 phase). Spectrum 12, 13 and 16, light gray regions, are the sections where Cu is concentrated (Cu-rich FCC2 phase). On the other hand, spectrum 9 and 10 are light-colored regions where Mo concentration is high in weight (μ phase). Similar EDX results with three different compositions are seen in $(\text{CoCuFeNi})_{100-x}\text{Mo}_x$ at% ($x = 15, 19$, and 25) alloys [8]. In addition, the elemental composition of the μ phase in this study as a result of EDX is

very close to that of the $\text{CoCrFeNiMo}_{0.2}$ alloy, which contains Co instead of Cu [27]. The SEM and EDX results in this study are consistent with XRD analysis.

The microhardness values obtained as a result of measurements taken from 5 different points are given in Table 1. It is expected that the hardness of the Mo-containing phase is highest while the hardness of Cu-rich phase is lowest. In a study on high entropy alloy [28], hardness increased as Mo content increased. In the literature [8], the microhardness value of the Mo-free CoCuFeNi alloy is 162 HV, while the microhardness value of the $(\text{CoCuFeNi})_{75}\text{Mo}_{25}$ alloy is 518 HV.

The coefficient of friction curve of CoCuFeNiMo alloy with different loads as a function of time under dry sliding is shown in Fig. 4. The coefficient of friction under a load of 12.5 N has a very stable curve. The coefficient of friction under 25 N load became stable at the end of 250 sec. However, a slight decrease was observed between 1250 sec and 1500 sec. On the other hand, there is a significant instability/fluctuation in the friction coefficient under 50 N load up to approximately 750 sec. This fluctuation resolved after approximately 750 sec and reached a stable state. This fluctuation in the coefficient of friction under 50 N load may be related to phase composition, inhomogeneity in the microstructure of the alloy, crack formations on the worn surface, oxidation or delamination layers formation [29]. Since there was no change in phase composition in this study, no effect can be considered. However, inhomogeneity in the microstructure may occur due to the segregation of the Cu element in the structure. This inhomogeneity may have appeared on the surface during wear under 50 N load. In addition, as the load increases, the interaction between the two surfaces will increase, and the appearance of wear debris, oxide layer and local cracks on the surface of the alloy may cause this fluctuation. Therefore, the coefficient of friction of the CoCuFeNiMo alloy increased as the load amount increased. In a study systematically examining the effects of Mo content on the microstructure, mechanical and tribological properties of CrCoNiMo_x alloys, there was no change in the friction coefficient as the amount of

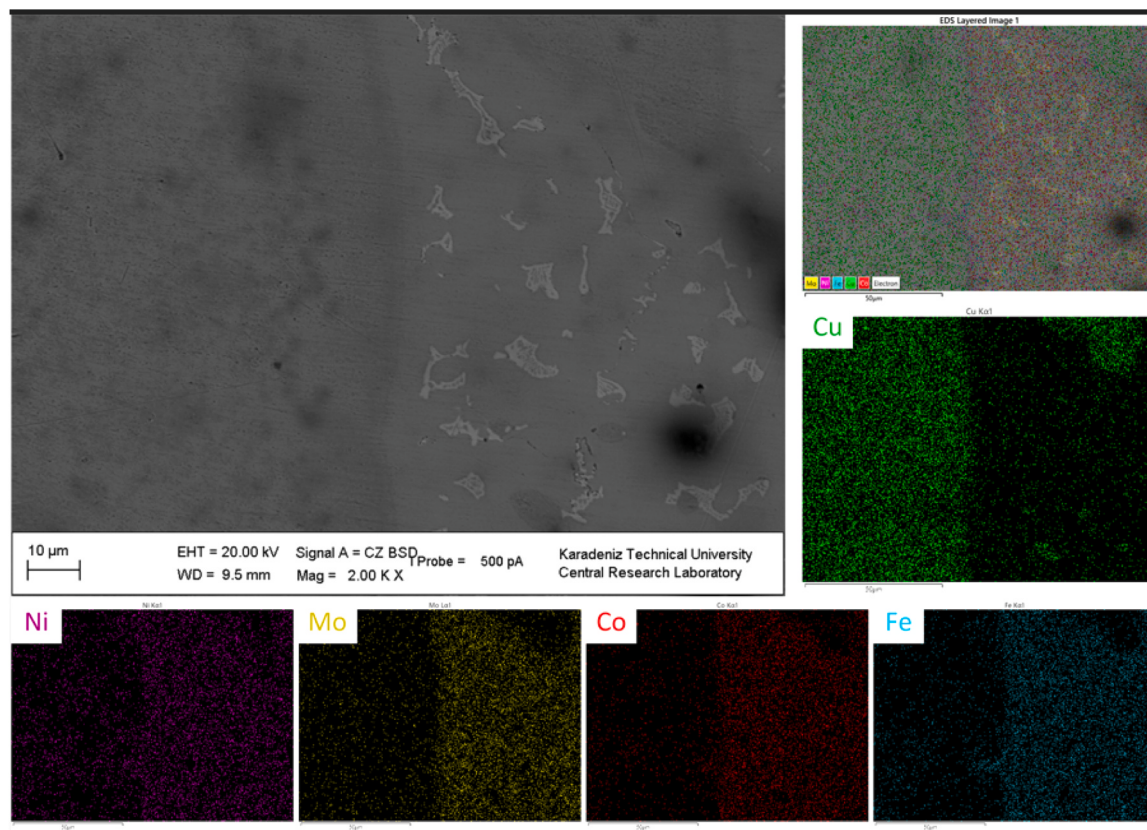


Fig. 2. SEM and mapping analysis of CoCuFeNiMo high entropy alloy.

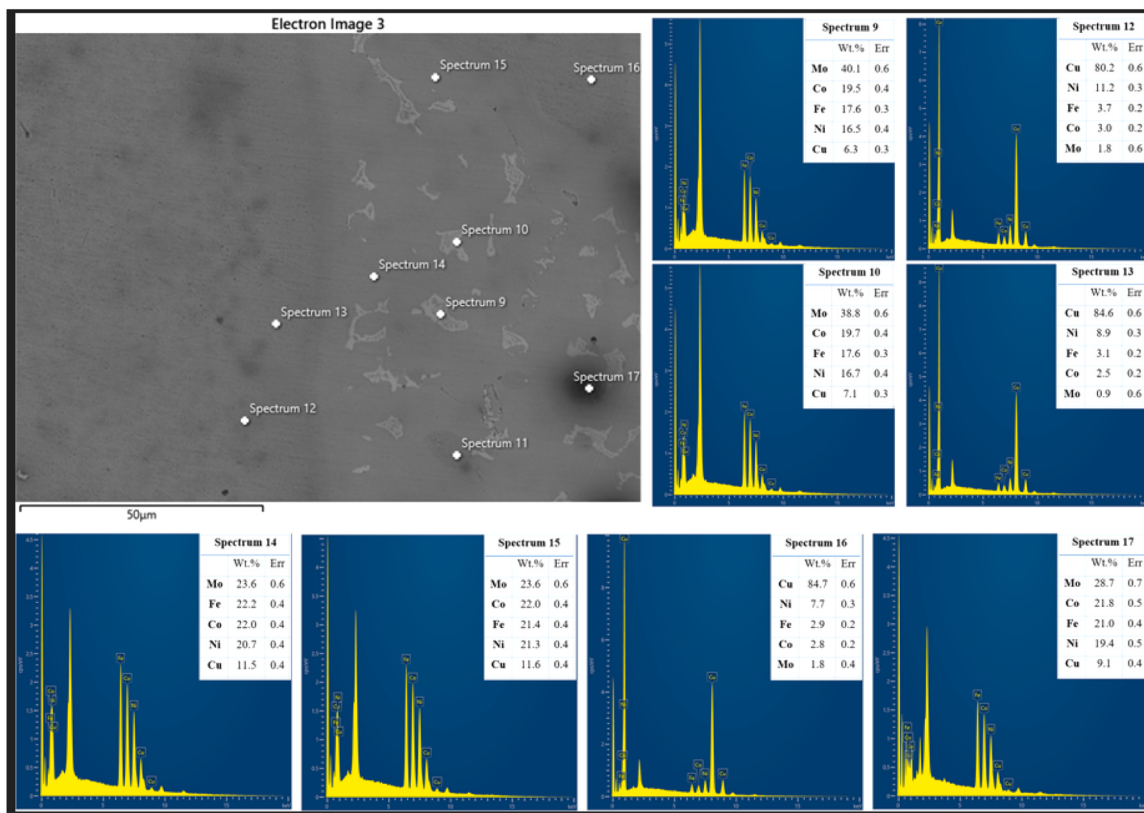


Fig. 3. EDX point results on the microstructure of CoCuFeNiMo high entropy alloy.

Table 1

Microhardness of three different structures in the microstructure of CoCuFeNiMo high entropy alloy.

Structure	Microhardness value ($\text{HV}_{0.1}$)
FCC1 phase	265 \pm 7
FCC2 phase (Cu-rich)	136 \pm 16
μ phase (Mo-rich)	364 \pm 28

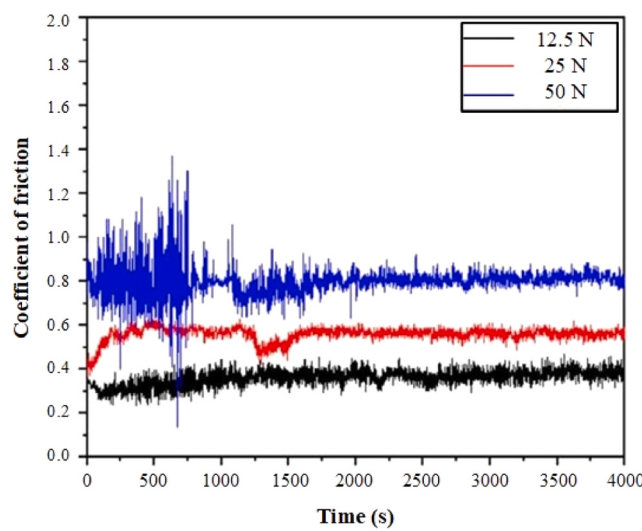


Fig. 4. Friction coefficient graph under 12.5 N, 25 N and 50 N loads of CoCuFeNiMo high entropy alloy.

Mo increased, and the friction coefficient was found to be approximately 0.6 [28].

Fig. 5 presents the weight losses and the wear rates versus the applied load. Upon varying loads, both weight loss and wear rate exhibit a monotonic increase. When the load increased from 12.5 N to 25 N, both weight loss and wear rate increased slightly. While weight loss increased from 0.0490 g to 0.0998 g, wear rate increased from $1.088 \times 10^{-4} \text{ mm}^3/\text{N.m}$ to $1.108 \times 10^{-4} \text{ mm}^3/\text{N.m}$. On the other hand, when it increased from 25 N to 50 N, the weight loss reached 0.2109 g, while the wear rate was found to be $1.171 \times 10^{-4} \text{ mm}^3/\text{N.m}$. These data indicate that the wear rate increases as the applied load increases, and therefore, there is a linear relationship in the wear properties of the alloy. This effect can be attributed to three factors: (1) the augmentation of

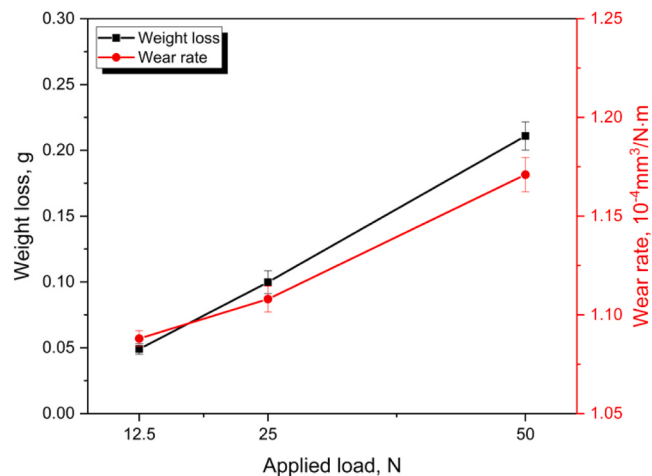


Fig. 5. Weight losses and wear rates of the CoCuFeNiMo high entropy alloy after wear tests applied different loads.

interlocking between surface irregularities, (2) the occurrence of oxidation, and (3) the softening, plastic deformation, and fracture of the material, similar to what is discussed in the Ref [30].

Fig. 6.a-f shows the worn surfaces of CoCuFeNiMo alloy at different loads. Features like delaminations, plowing, abrasive wear tracks and some wear debris, which are characteristics of dry sliding wear, are clearly visible. Surprisingly, a similar worn surface morphology was observed. Their wear mechanism can be considered mild abrasive wear. Abrasive wear is a common mechanism around high entropy alloys [31]. This phenomenon occurs due to the dislodgment of debris from the worn surface and the transfer of adhering particles onto the surface of the hard material. This process induces a plowing effect on the soft metal during wear [32]. Notably, the worn surface in the vicinity of the grooves remains relatively undisturbed. As the load increases, the formation of oxide and delamination also increases. Loss of continuity and occurred damage, especially at high loads, on the surface caused an increase in wear loss. In addition, increasing the amount of load increases the surface contact area. The plateaus formed due to the contact area on the surface of the CoCuFeNiMo alloy are exposed to large contact stress. Also, the local temperature on the surface increases as a result of the frictional heat caused by sliding. In addition to the increase in temperature, oxide layers may form as a result of the chemical interactions of the protruding parts on the surface with the air (Fig. 6.f).

To examine the corrosion behavior of the CoCuFeNiMo alloy, a

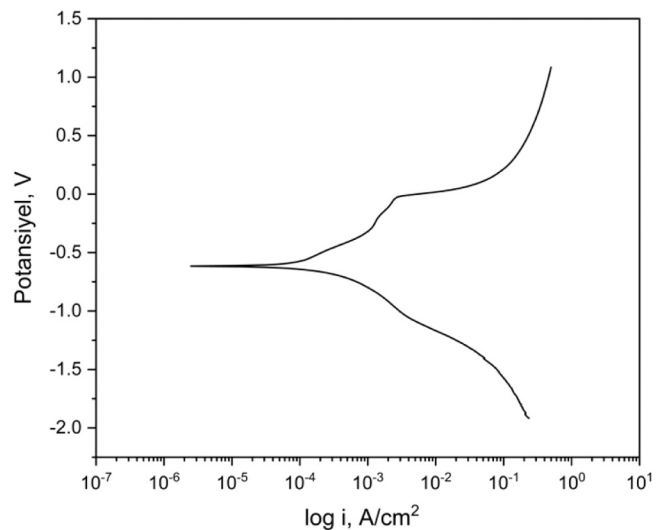


Fig. 7. Tafel polarization curves.

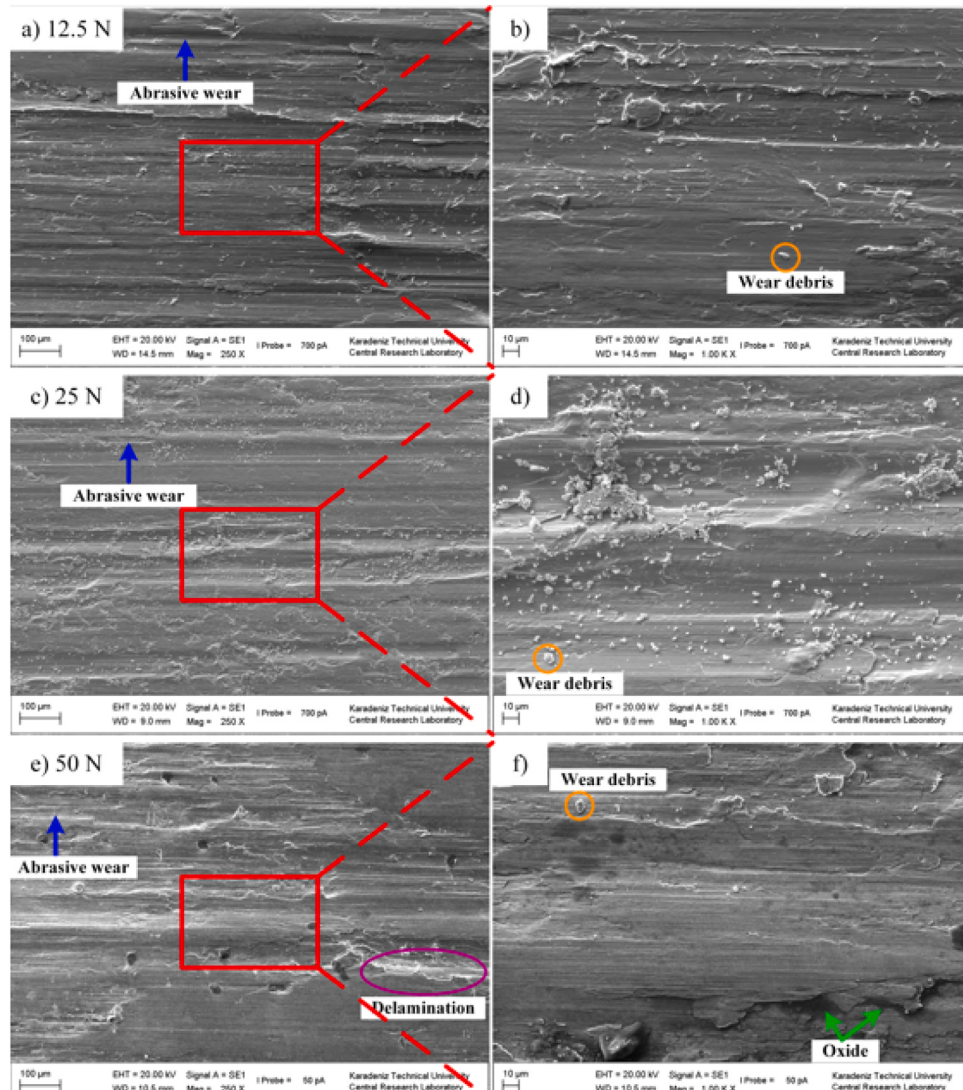


Fig. 6. SEM morphologies of worn surfaces of CoCuFeNiMo high entropy alloy under (a) and (b) 12.5 N, (c) and (d) 25 N, (e) and (f) 50 N loads.

potentiodynamic polarization curve conducted in a 3.5 wt% NaCl aqueous solution at room temperature is illustrated in Fig. 7. The Ecorr value is -0.616 V, and the icorr value is 2.22×10^{-5} A/cm². While the Ecorr reflects only the corrosion tendency, the icorr represents the corrosion rate, with higher icorr values indicating greater corrosion rates for the alloys. Similar curves have been reported in previous studies [33–35], and comparable corrosion values can be found in the literature [36–38].

In the cathodic zone, the current density decreases as the potential rises, aligning with the cathodic reaction associated with the oxygen evolution process [39]. With further voltage increase, the sample undergoes an anodic dissolution process, leading to a sudden surge in the self-corrosion current density [40]. Subsequently, as the voltage continues to rise, the self-corrosion current density gradually stabilizes, transitioning into the passive zone. Upon further voltage escalation, the self-corrosion current density rises again, entering the transpassive zone. The anodic portion of the curve reveals critical characteristics related to the material's corrosion resistance [34].

The surface morphologies of the alloys after the potentiodynamic polarization tests are given in Fig. 8. Backscattered electrons (BSD) mode of secondary electrons (SE1) mode of SEM images are presented in Fig. 8.a,b and Fig. 8.c,d, respectively. It is evident that the corrosion attack, which pitted corrosion, was localized in both image modes. The corrosion morphologies observed in the CoCuFeNiMo alloy displayed features of uniform corrosion without any signs of selective corrosion damage. The reason for the formation of pitting corrosion is the attack of Cl⁻ ions. Some pitting pits with a size of approximately 4 μm were seen in Fig. 8.b. The electrochemical corrosion process is thought to occur as follows: Firstly, small cavities are formed at inhomogeneous grain boundaries. These small cavities gradually grew and merged with other small cavities. Secondly, tiny pits continue to form in the subgrains, and the subgrains begin to dissolve. This cycle continues continuously, and large-sized pits are formed [41]. Additionally, black corrosion products appear to form at the grain boundaries between the μ phase and the FCC phase. As a result, nonuniform corrosion eventually resulted. This corrosion type can be described as galvanic corrosion.

Fig. 9 shows the Nyquist curve (Fig. 9.a) and Bode and phase angle curves (Fig. 9.b) of the CoCuFeNiMo alloys in 3.5 wt% NaCl solution at room temperature. The Nyquist plot depicted an incomplete semicircle, implying that the corrosion event with a single time constant was predominantly influenced by the charge transfer process[42]. This indicates that a larger semicircular radius corresponds to increased charge transfer resistance and a more robust protective passive film. The Bode plot illustrates a linear correlation between the logarithm of |Z| and the logarithm of |f| within the frequency range of 10^{-2} to 10^3 Hz. The electrochemical behavior of the samples was simulated using the electrical equivalent circuit (EEC) depicted in Fig. 9.c. The fitting outcomes are highly satisfactory, supporting the validity of the two-layer assumption for the oxide film developed on the CoCuFeNiMo to a considerable extent. Within the circuit, Rsol identifies the solution resistance, Rpo and Cc represent the resistance and capacitance of the outer layer. At the same time, Rcor and Ccor correspond to the resistance and capacitance of the inner layer. To tackle non-uniformity within the system, the constant phase element parameter C is employed, adhering to a conventional approach in circuit analysis. Table 2 lists major fitting parameters obtained from CoCuFeNiMo alloy after polarization. A similar Nyquist, Bode diagram and circuit formation is seen in the corrosion of high entropy alloys in the literature [43].

4. Conclusions

This study was conducted to evaluate the structural, wear, and corrosion properties of the CoCuFeNiMo high-entropy alloy. The XRD analysis revealed that the alloy consists of predominantly two FCC phases and slightly a (μ) phase. Fluctuations in the friction coefficient were observed under a 50 N load, and these fluctuations were associated with potential microstructural homogeneity deficiencies or the segregation of Cu within the structure. Wear tests were performed under various loads, and the determined wear rates are as follows: 1.111×10^{-4} mm³/N.m at 12.5 N load, 1.124×10^{-4} mm³/N.m at 25 N load, and 1.211×10^{-4} mm³/N.m at 50 N load. These results indicate an increase in wear resistance with the applied load. Mild abrasive marks

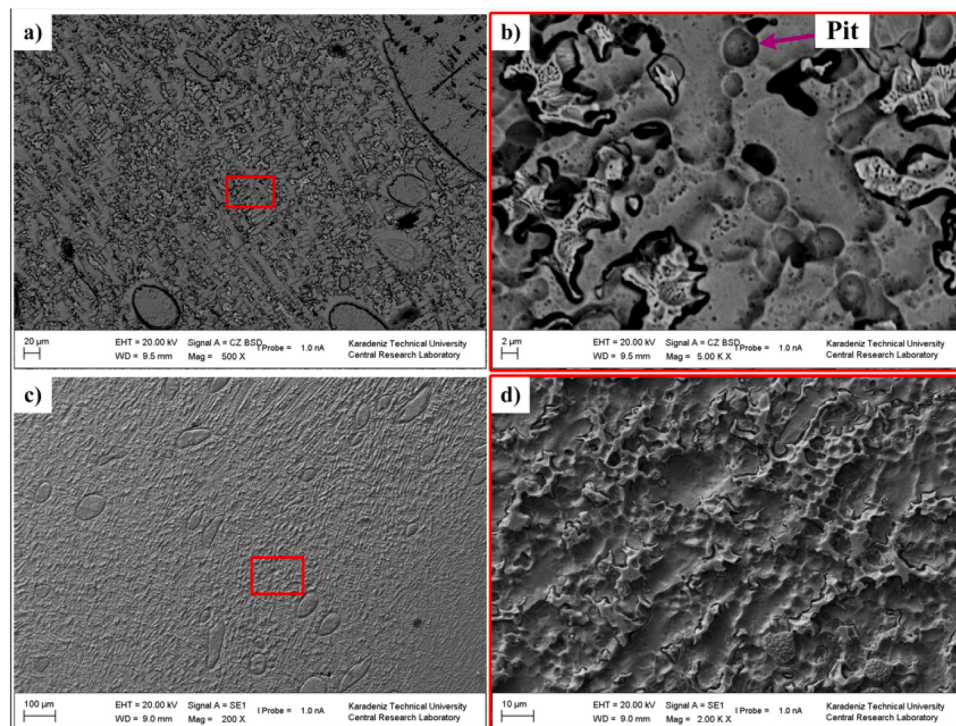


Fig. 8. Corrosion surfaces after tafel measurement.

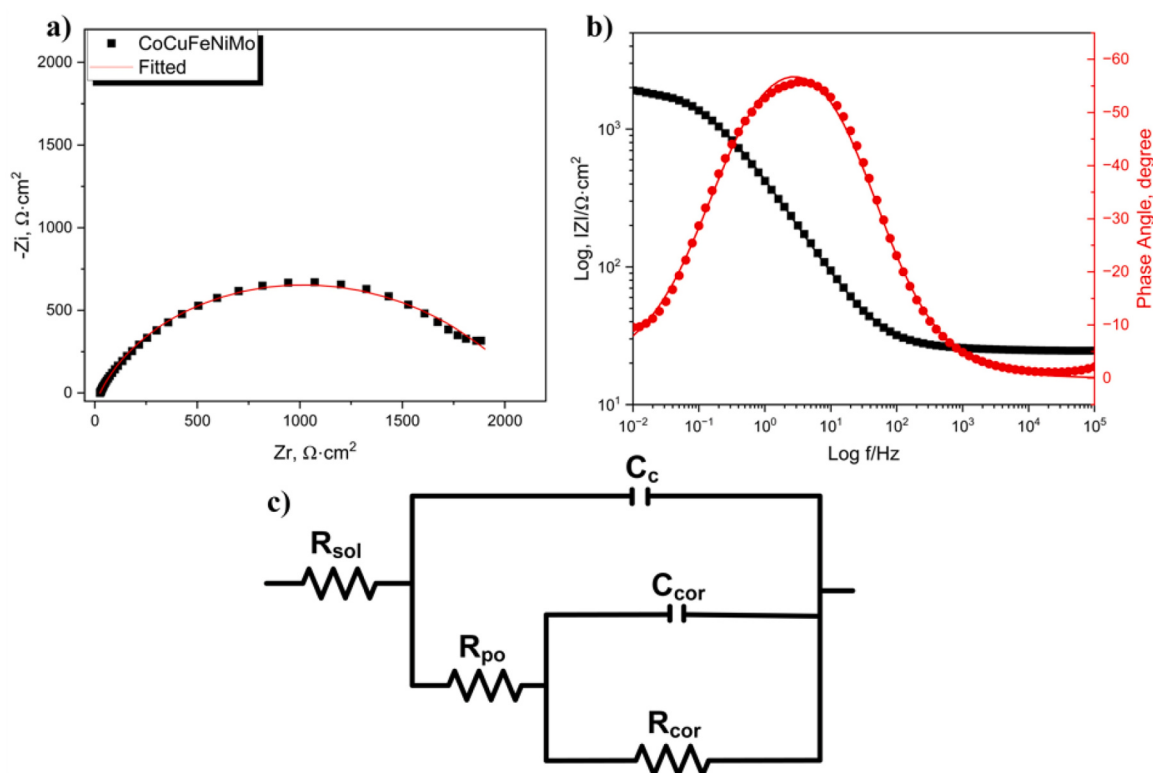


Fig. 9. a) Nyquist curve, b) Bode and phase angle curve of CoCuFeNiMo alloy and c) Equivalent electrical circuit used to fit the EIS data.

Table 2

Equivalent circuit fitting parameters for EIS of CoCuFeNiMo alloy in 3.5 wt% NaCl solution.

Parameter	Value	±Error	Units
R_{sol}	25.02	155.2e-3	$\Omega \cdot \text{cm}^2$
R_{cor}	608.1	4.319e3	$\Omega \cdot \text{cm}^2$
R_{po}	1.559e3	3.415e3	$\Omega \cdot \text{cm}^2$
C_{cor}	1.564e-3	21.99e-3	$\Omega^{-1} \cdot \text{cm}^{-2} \cdot \text{s}^n$
n	311.7e-3	1.607	-
C_c	524.2e-6	47.12e-6	$\Omega^{-1} \cdot \text{cm}^{-2} \cdot \text{s}^n$
m	764.7e-3	14.81e-3	-
Goodness of Fit	6.167e-3	-	-

and delamination layers were observed on the worn surfaces. Corrosion behavior was investigated through potentiodynamic polarization tests and electrochemical impedance spectroscopy. The E_{corr} (corrosion potential) value was -0.616 V, and the I_{corr} (corrosion current) value was determined as 2.22×10^{-5} A/cm². Finally, the CoCuFeNiMo alloy demonstrated relatively high wear resistance, and the wear rate values determined at different loads support this observation. The alloy also exhibited resistance to corrosive environments, making it potentially suitable for various industrial applications. However, further research is needed to understand the influence of Cu segregation on friction behavior. These findings contribute significantly to understanding and optimizing the potential of high-entropy alloys in engineering applications.

Declaration of Competing Interest

The authors declare that they have no known competing financial interests or personal relationships that could have appeared to influence the work reported in this paper.

Data availability

Data will be made available on request.

Acknowledgments

The author would like to thank Dr. Kürşat İçin, assistant principal of Manyetam and faculty member of the Department of Metallurgical and Materials Engineering in Karadeniz Technical University, for his valuable contributions and thank Ömer Şahin, lecturer at Gazi University for microhardness measurements.

References

- [1] B. Cantor, I.T.H. Chang, P. Knight, A.J.B. Vincent, Microstructural development in equiatomic multicomponent alloys, *Mater. Sci. Eng.: A* 375–377 (2004) 213–218.
- [2] J.-W. Yeh, S.-K. Chen, S.-J. Lin, J.-Y. Gan, T.-S. Chin, T.-T. Shun, C.-H. Tsau, S.-Y. Chang, Nanostructured high-entropy alloys with multiple principal elements: novel alloy design concepts and outcomes, 6 (2004) 299–303.
- [3] J.W. Choi, J.T. Kim, S.H. Hong, H.J. Park, E. Jumaev, K.B. Kim, Investigation of correlation between the microstructural characteristics and mechanical properties of (CoCuFeNi)100-xAlx high entropy alloys, *J. Alloy. Compd.* 933 (2023) 167679.
- [4] T.M. Ribeiro, E. Catellani, A. Garcia, C.A. dos Santos, The effects of Cr addition on microstructure, hardness and tensile properties of as-cast Al-3.8wt%Cu-(Cr) alloys, *J. Mater. Res. Technol.* 9 (2020) 6620–6631.
- [5] A. Verma, P. Tarate, A.C. Abhyankar, M.R. Mohape, D.S. Gowtam, V.P. Deshmukh, T. Shanmugasundaram, High temperature wear in CoCrFeNiCu high entropy alloys: the role of Cu, *Scr. Mater.* 161 (2019) 28–31.
- [6] D.G. Kim, Y.H. Jo, J.M. Park, W.-M. Choi, H.S. Kim, B.-J. Lee, S.S. Sohn, S. Lee, Effects of annealing temperature on microstructures and tensile properties of a single FCC phase CoCuMnNi high-entropy alloy, *J. Alloy. Compd.* 812 (2020) 152111.
- [7] X. Sun, H. Zhu, J. Li, J. Huang, Z. Xie, High entropy alloy FeCoNiCu matrix composites reinforced with in-situ TiC particles and graphite whiskers, *Mater. Chem. Phys.* 220 (2018) 449–459.
- [8] Y. Shao, H. Ma, Y. Wang, Effect of Mo addition on the microstructure and mechanical properties of CoCuFeNi high entropy alloy, 10 (2020) 1017.
- [9] H. Qiu, H. Zhu, J. Zhang, Z. Xie, Effect of Fe content upon the microstructures and mechanical properties of FeCoNiCu high entropy alloys, *Mater. Sci. Eng.: A* 769 (2020) 138514.

- [10] D. Bae, H. Choi, J.Y. Hwang, J. Jeon, M.J. Kim, J.-H. Kim, S. Nam, J. Park, Deformation behavior of nanocrystalline and ultrafine-grained CoCrCuFeNi high-entropy alloys, *J. Mater. Res.* 34 (2019) 720–731.
- [11] X. Qiu, Microstructure and mechanical properties of CoCrFeNiMo high-entropy alloy coatings, *J. Mater. Res. Technol.* 9 (2020) 5127–5133.
- [12] A. Kumar, A. Singh, A. Suhane, A.K. Singh, P.K. Verma, Wear and corrosion behavior of high entropy alloys, *Mater. Today.: Proc.* (2023).
- [13] J.-K. Xiao, G.-M. Xu, J. Chen, P. Rasinov, C. Zhang, Tribocorrosion behavior of TiZrHfNb-based refractory high-entropy alloys, *Wear* 536–537 (2024) 205158.
- [14] H. Ren, R.R. Chen, X.F. Gao, T. Liu, G. Qin, S.P. Wu, J.J. Guo, High-performance AlCoCrFeNi high entropy alloy with marine application perspective, *J. Mater. Res. Technol.* 25 (2023) 6751–6763.
- [15] X. Zhang, Y. Yu, T. Li, L. Wang, Z. Qiao, Z. Liu, W. Liu, Effect of the distribution of Cu on the tribocorrosion mechanisms of CoCrFeNiCu0.3 high-entropy alloys, *Tribol. Int.* 193 (2024) 109401.
- [16] Y. Sun, Z. Wang, W. Wang, X. Zhao, K. Zhu, H. Li, Y. Zhao, Z. Yin, Wear and corrosion resistance of Al1.2CoCrFeNiScx high entropy alloys with scandium addition, *J. Mater. Res. Technol.* 27 (2023) 8023–8036.
- [17] J. Wang, W. Wen, J. Cheng, L. Dai, S. Li, X. Zhang, Y. Yang, H. Li, X. Hou, B. Wu, J. Wu, Tribocorrosion behavior of high-entropy alloys FeCrNiCoM (M = Al, Mo) in artificial seawater, *Corros. Sci.* 218 (2023) 111165.
- [18] J. Miao, H. Liang, A. Zhang, J. He, J. Meng, Y. Lu, Tribological behavior of an AlCoCrFeNi2.1 eutectic high entropy alloy sliding against different counterfaces, *Tribol. Int.* 153 (2021) 106599.
- [19] J. Miao, H. Yao, J. Wang, Y. Lu, T. Wang, T. Li, Surface modification for AlCoCrFeNi2.1 eutectic high-entropy alloy via laser remelting technology and subsequent aging heat treatment, *J. Alloy. Compd.* 894 (2022) 162380.
- [20] F. Ge, H. Yuan, Q. Gao, T. Peng, S. Guo, P. Lyu, Q. Guan, H. Liu, X. Liu, J. Guan, Microstructure, hardness and wear resistance of AlCoCrFeNiTax ($x = 0, 0.1, 0.3$) high-entropy alloys enhanced by laser remelting and Ta addition, *J. Alloy. Compd.* 949 (2023) 169741.
- [21] B. Shi, D. Xin, X. Chen, Y. Wang, A. Singh, Fabrication of high-strength dual FCC phase Co-Cr-Fe-Ni-Cu-Mo high entropy alloy by plasma arc additive manufacturing using a combined cable wire, *Mater. Lett.* 337 (2023) 133983.
- [22] Q. Wu, Z. Wang, F. He, J. Li, J. Wang, Revealing the selection of σ and μ phases in CoCrFeNiMo high entropy alloys by CALPHAD, *J. Phase Equilibria Diffus.* 39 (2018) 446–453.
- [23] X. Li, Z. Li, Z. Wu, S. Zhao, W. Zhang, H. Bei, Y. Gao, Strengthening in Al-, Mo- or Ti-doped CoCrFeNi high entropy alloys: a parallel comparison, *J. Mater. Sci. Technol.* 94 (2021) 264–274.
- [24] T.-T. Shun, L.-Y. Chang, M.-H. Shiu, Microstructure and mechanical properties of multiprincipal component CoCrFeNiMo alloys, *Mater. Charact.* 70 (2012) 63–67.
- [25] J.W. Bae, J.M. Park, J. Moon, W.M. Choi, B.-J. Lee, H.S. Kim, Effect of μ -precipitates on the microstructure and mechanical properties of non-equiautomic CoCrFeNiMo medium-entropy alloys, *J. Alloy. Compd.* 781 (2019) 75–83.
- [26] V.K. Soni, S. Sanyal, S.K. Sinha, Phase evolution and mechanical properties of novel FeCoNiCuMo high entropy alloys, *Vacuum* 174 (2020) 109173.
- [27] F. He, Z. Wang, B. Han, Q. Wu, D. Chen, J. Li, J. Wang, C.T. Liu, J.J. Kai, Solid solubility, precipitates, and stacking fault energy of micro-alloyed CoCrFeNi high entropy alloys, *J. Alloy. Compd.* 769 (2018) 490–502.
- [28] J. Miao, T. Guo, J. Ren, A. Zhang, B. Su, J. Meng, Optimization of mechanical and tribological properties of FCC CrCoNi multi-principal element alloy with Mo addition, *Vacuum* 149 (2018) 324–330.
- [29] H. Wu, S. Zhang, Z.Y. Wang, C.H. Zhang, H.T. Chen, J. Chen, New studies on wear and corrosion behavior of laser cladding FeNiCoCrMox high entropy alloy coating: the role of Mo, *Int. J. Refract. Met. Hard Mater.* 102 (2022) 105721.
- [30] T.R. Prabhu, M. Arivaraasu, Y. Chodancar, N. Arivazhagan, G. Sumanth, R. K. Mishra, Tribological behaviour of graphite-reinforced FeNiCrCuMo high-entropy alloy self-lubricating composites for aircraft braking energy applications, *Tribol. Lett.* 67 (2019) 78.
- [31] P.J. Mane, M. Shanmharaja, B. Manne, B.S. Raju, Effect of FeCoNiMnCr high-entropy alloy reinforcement on mechanical, wear, and thermal expansion behavior of copper matrix composites, *JOM* 75 (2023) 4421–4434.
- [32] Z. Li, X. Wang, Y. Huang, Z. Xu, Y. Deng, X. Jiang, X. YangMicrostructure, mechanical property, and wear behavior of NiAl-based high-entropy alloy, 13, 2023. 1737..
- [33] L. Huang, X. Wang, X. Zhao, C. Wang, Y. Yang, Analysis on the key role in corrosion behavior of CoCrNiAlTi-based high entropy alloy, *Mater. Chem. Phys.* 259 (2021) 124007.
- [34] Y. Li, Y. Shi, R. Chen, H. Lin, X. Ji, Corrosion behavior and comprehensive evaluation of Al0.8CrFeCoNiCu0.5B0.1 high-entropy alloy in 3.5% NaCl solution, 11 (2023) 282.
- [35] S. Yang, W. Yu, T. Liu, C. Li, Y. Zhang, Y. Qu, Effect of Cr content on corrosion behavior of AlCrxFeNi2Cu1.6 high entropy alloys, *Mater. Res. Express* 6 (2019) 076501.
- [36] C.-C. Yen, S.-Y. Lin, C.-L. Ting, T.-L. Tsai, Y.-T. Chen, S.-K. Yen, Passivation mechanisms of CoCrFeNiMox ($x = 0, 0.1, 0.2, 0.3$) high entropy alloys and MP35N in 3.5 wt% NaCl aerated aqueous solutions, *Corros. Sci.* 228 (2024) 111812.
- [37] Q. Wang, A. Amar, C. Jiang, H. Luan, S. Zhao, H. Zhang, G. Le, X. Liu, X. Wang, X. Yang, J. Li, CoCrFeNiMo0.2 high entropy alloy by laser melting deposition: Prospective material for low temperature and corrosion resistant applications, *Intermetallics* 119 (2020) 106727.
- [38] M. Navazani, S.R. Kada, D. Fabijanic, M. Barnett, Increasing ductility via Cu addition in AlxCrFeMnNi: Towards a scrap-based high entropy alloy, *Intermetallics* 164 (2024) 108100.
- [39] H. Abe, T. Kobayakawa, H. Maruyama, T. Wakabayashi, M. Nakayama, Thin film coating of Mg-intercalated layered MnO₂ to suppress chlorine evolution at an IrO₂ anode in cathodic protection, *Electrocatalysis* 10 (2019) 195–202.
- [40] S. Wang, X.-y Zhou, M. Chi-Yuan, B. Long, H. Wang, J.-J. Tang, J. Yang, Electrochemical properties of Pb-0.6 wt% Ag powder-pressed alloy in sulfuric acid electrolyte containing Cl⁻/Mn²⁺ ions, *Hydrometallurgy* 177 (2018) 218–226.
- [41] Z. Wang, J. Zhu, Y. Guo, W. Xin, X. Hui, Y. Wu, H. Zheng, Y. Zhao, X. Wang, Multi-effects of Mo on enhancement of wear and corrosion resistances of FeCoNiCrMox high entropy alloys coatings prepared by laser powder directed energy deposition, *Surf. Coat. Technol.* 477 (2024) 130378.
- [42] K. Wang, Y. Zhu, P.-w Wang, X. Li, B. Malomo, L. Yang, Enhancing corrosion resistance in CoCrFeNiTa high entropy alloys via Mo addition, *Electrochim. Acta* 480 (2024) 143951.
- [43] X. Wan, A. Lan, M. Zhang, X. Jin, H. Yang, J. Qiao, Corrosion and passive behavior of Al0.8CrFeNi2.2 eutectic high entropy alloy in different media, *J. Alloy. Compd.* 944 (2023) 169217.